PIV measurements in co–flowing jets subjected to axial forcing. Vorticity and strain field structure

by

U. Ruiz-Rivas, A. Lecuona, P. Rodriguez and J. Nogueira

Escuela Técnica Superior
Universidad Carlos III de Madrid
Avda. Universidad 30, 28913 Leganés, Spain
E-mail: ulpiano@ing.uc3m.es

ABSTRACT

A study of the evolving shear layer in the near field of Re_D=7000, co–flowing water jets is presented. The inner jet is subjected to a strong axial forcing and to a small, controlled azimuthal perturbation. This flow configuration is characterised by a strong lateral expansion of the inner jet in the near field, controlled by the forcing parameters. Instantaneous, whole-field, 2D velocity measurements using the Digital Particle Image Velocimetry (DPIV) technique. The 2D, two-component velocity measurements allows for the computation of fields of azimuthal vorticity and strain. These parameters control the inviscid dynamics of the structures of azimuthal vorticity that dominates the near field evolution of the flow. The vorticity and strain fields for one of the phase-locked DPIV measurement obtained are shown in figure 1. The pressure distribution is also investigated. The combined information of these flow parameters provides a deep insight in the flow nature and evolution.

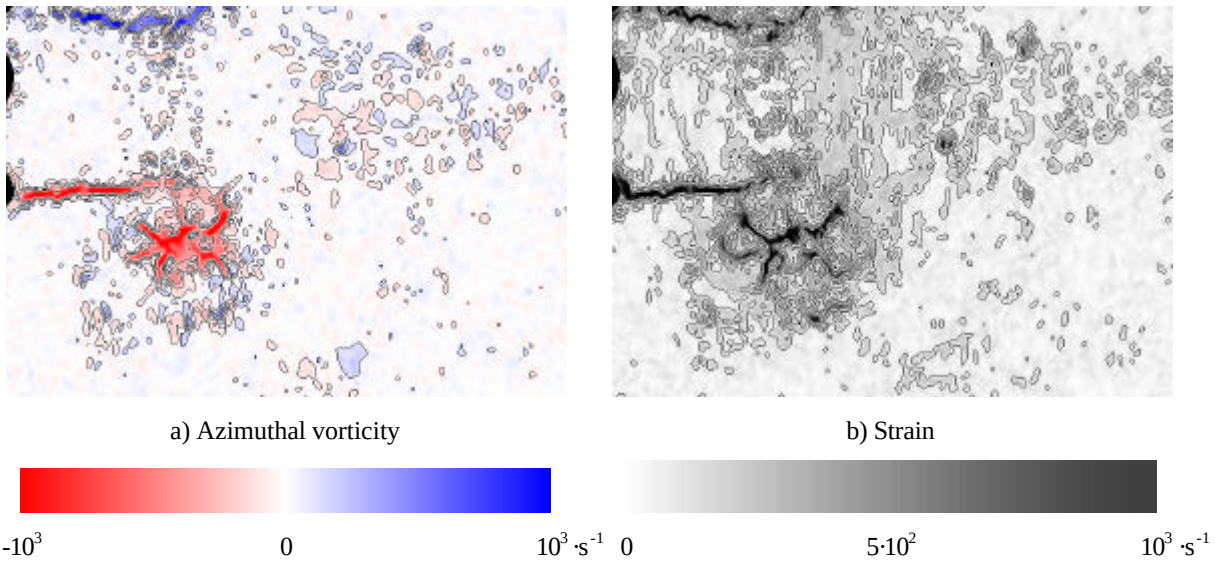

Figure 1. *Vorticity field and strain field calculated from a DPIV velocity map. Flow comes from left to right. The nozzle exit lobes can be seen on the upper left side.*

1. INTRODUCTION

The flow of forced co-flowing jets was first studied by Lasheras et al (1992). The flow configuration is of industrial interest in applications such us combustors, mixers, etc. Also, Monkiewitz and co-workers (for example, Monkiewitz and Pfizenmaier (1991)) compared the flow evolution of strongly forced jets to that of self-excited jets, in which the excitation is due to a temperature or density difference between the jet and its surrounding atmosphere. Several other authors, as Grinstein et al (1996), Brancher et al (1994), etc. have studied similar flows, either numerically or experimentally.

Inn a previous study, Rodríguez et al (2000) studied the three-dimensional structure of the vorticity field in laminar (Re_D=400) co-flowing air jets, using flow visualisation techniques. In this paper a more complete view of the flow is given, by means of PIV measurements of the velocity field in longitudinal planes of the flow.

The main characteristics observed in the laminar studies can be extrapolated to the higher Reynolds number flow presented here, due to the inviscid nature of the near-field evolution of the flow. Therefore, it is interesting to resume the main results of the afore-mentioned laminar studies.

The axial forcing produces a considerable change in the near field topology of the flow. The well-known axial instability is locked to the forcing frequency and enhanced considerably, so the primary structure of equi-spaced vortex rings appears already at the surroundings of the nozzle exit. The azimuthal perturbation locks the azimuthal (or secondary) instability wavenumber, and the strong strain field due to the vortex rings amplifies the developing secondary structure. Finally, a third vortex structure appears, due to vortex induction of suction velocities in the surroundings of the nozzle rim. This third structure also develops an azimuthal organisation, which is affected by the azimuthal perturbation. The interaction of this third structure of counter-rotating vortex rings and the primary structure of concentrated vortex rings produces the distortion and re-location of the counter-rotating vortices. It is shown that the observed evolution follows inviscid dynamics mechanisms. All these complex three-dimensional interactions lead to the enhancement of the lateral expansion of the inner jet. These processes are explained in Rodríguez et al (2000).

2. EXPERIMENTAL FACILITY

The experiments were conducted in a horizontal water tunnel of the closed type. A scheme of the tunnel is shown in figure 2. It consists of two independently created, low speed streams, whose velocities can be independently controlled. The inner stream is produced through a round nozzle of an inner diameter D = 15 mm, located downstream of a settling chamber. A slower, co-flowing stream of square cross section surrounds the inner jet. The two streams meet in a box of 200x200 mm square cross-section, which has lateral walls of transparent metacrilate. The flow is evacuated through two lateral apertures at the end of the box. The configuration is chosen to avoid re-circulation as a result of jet entrainment. The end wall is constructed of transparent metacrilate, providing a zenithal viewpoint of the flow, which was used for flow visualisation.

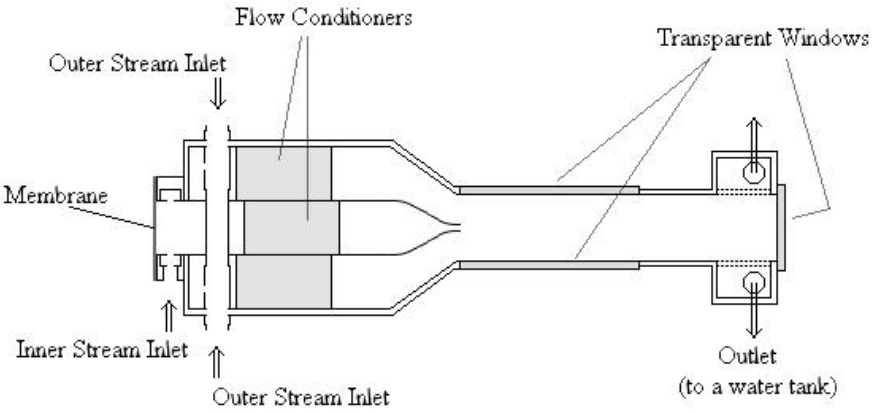

Figure 2. *Scheme of the flow facility.*

The periodic axial forcing is produced through a vibrating membrane located at the upstream end of the settling chamber of the inner flow, driven by a loudspeaker fed with a sinusoidal wave. The membrane motion adds an axial velocity monochromatic fluctuation of a given amplitude and frequency to the inner jet flow. The azimuthal perturbation was introduced by using a 5-lobes indented nozzle exit lip. The sinusoidal profile had ±1.5 mm amplitude.

The relevant dimensionless parameters of the flow are the Reynolds number, *Re*, the Strouhal number, *St* (defined over the axial forcing frequency, *f*), the amplitude of the axial forcing, A_z, and the velocity ratio between inner and outer flow, u_R. For the above exposed conditions, the dimensionless parameters have the following values:

$$Re = \frac{(u_{i,mean} - u_o)D}{n} = 7000 \qquad St = \frac{fD}{(u_{i,mean} + u_o)/2} \text{ varies from 0.4 to 1.5}$$

$$A_z = \frac{u_{i,max} - u_{i,min}}{u_{i,max} + u_{i,min}} \text{ varies from 0 to 1} \qquad u_R = \frac{u_{i,mean} - u_o}{u_{i,mean} + u_o} = 0.37$$

A scheme of the experimental system can be seen in figure 3. Two PC's control the whole system. PC I controls the acquisition process through a processor. The processor maintains the synchronisation between the camera and the illuminating system, which is constituted by two aligned Nd-YAG lasers, a beam guide and a cylindrical lens. PC II generates the forcing signal, which feeds the loudspeaker through a power amplifier, controlling both frequency and amplitude of the forcing. PC II also triggers the PIV system through the processor to get phase locked measurements.

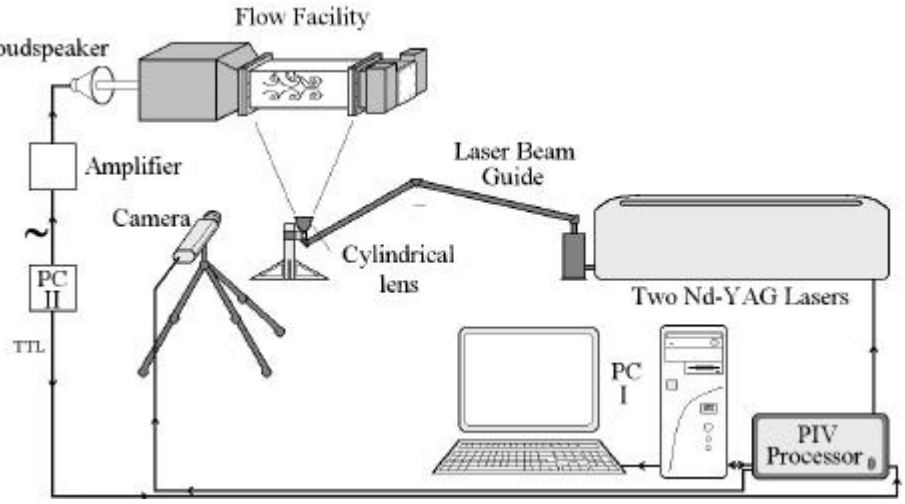

Figure 3. *Scheme of the measurement system*

For the PIV measurements, both the inner and outer flow were seeded with licopodium spores, which are barely mono-dispersed ($d_l \sim 20\mu m$) and neutrally buoyant. The Stokes number of the licopodium spores in the studied flow was around 10^{-3}, defined for the axial forcing frequency.

The measurements of the velocity field have been obtained using the DPIV technique. A commercial system (DANTEC FlowMap®) has been used for the acquisition of the images. Then, the processing has been done using a High Resolution PIV technique. The LFC PIV developed by Nogueira et al. (1998) was chosen for this task, giving satisfactory results. This advanced PIV processing method includes two improvements in respect to a traditional PIV system that makes it specially suited for the images here presented. On one hand, its high-resolution capability allows for the description of several small features of the flow even with the 768 by 484 pixels camera used. On the other, its capability to deal with large velocity gradients allows to obtain measurements in a flow-field presenting large vorticity and strain values; without the need to limit the time between PIV images to undesired small values.

The PIV measurements field of view was around 45x30 mm (3*Dx2D*), taken by a 768x484 pixels CCD sensor camera. The LFC PIV algorithm was carried out over areas of 64x64 pixels and with 4 pixels displacement between successive interrogation areas. Sub-pixel peak fitting was used. The LFC PIV method has built-in algorithms for validation and interpolation of erroneous vectors, but the incidence of such vectors was negligible in all cases (less than 1% of the obtained vectors). The time between illuminating pulses was 700μs.

Post-processing consisted on derivative calculation to obtain the vorticity and strain fields. The results here presented use the circulation filter (being the most widely used) for the derivatives. The circulation filter has the form:

$$\frac{\partial v_y}{\partial x} = \frac{1}{12}\frac{\left(v_{y\,(i+1,\ j+1)} + 4v_{y\,(i+1,\ j)} + v_{y\,(i+1,\ j-1)}\right) - \left(v_{y\,(i-1,\ j+1)} + 4v_{y\,(i-1,\ j)} + v_{y\,(i-1,\ j-1)}\right)}{\Delta x}$$

3. DERIVED PARAMETERS

The 2D PIV technique is applied over longitudinal cuts of the flow in its near field, obtaining the u_z, u_r velocity components of the velocity. Several variables can be derived from these measurements. Typically, the azimuthal component of the vorticity can be obtained by:

$$\vec{w}_q = \left(\frac{\partial v_r}{\partial z} - \frac{\partial v_z}{\partial r}\right)\vec{u}_q \qquad (1)$$

In order to obtain other parameters, several reasonable assumptions have to be made: the flow is considered to be incompressible and the measurements plane is a plane of symmetry of the flow. Therefore:

$$\nabla\cdot v = 0 \qquad v_q = 0 \qquad \frac{\partial v_r}{\partial q} = 0 \qquad \frac{\partial v_z}{\partial q} = 0 \qquad (2)$$

With such simplifications, the strain tensor can be reduced and its contraction can be obtained by:

$$s = \left(2s_{ij}s_{ij}\right)^{\frac{1}{2}} = \left[2\left(\frac{\partial v_r}{\partial r}\right)^2 + 2\left(\frac{\partial v_z}{\partial z}\right)^2 + \left(\frac{\partial v_r}{\partial z} + \frac{\partial v_z}{\partial r}\right)^2 + 2\left(\frac{\partial v_r}{\partial r} + \frac{\partial v_z}{\partial z}\right)^2\right]^{\frac{1}{2}} \qquad (3)$$

The information of the strain field is better presented as compared with the local azimuthal vorticity. Hence, a local coefficient, χ, has been defined as:

$$c = \frac{s^2 - w^2}{s^2 + w^2} \qquad (4)$$

Furthermore, some information about the pressure distribution over the measurement plane can be derived from the 2D PIV data. Bradshaw and Koh (1981) showed that in a incompressible flow the pressure changes are related with the strain and vorticity fields in the form:

$$-\frac{\nabla^2 p}{r} = \frac{s^2 - w^2}{2} \qquad (5)$$

4. RESULTS AND DISCUSION

The results here presented are derived from four PIV velocity maps obtained for equi-spaced phases along a forcing cycle. The flow is strongly forced ($A_z = 0.9$) with a low frequency ($f = 10$Hz, giving a Strouhal number, $St = 0.45$). The low Strouhal number indicates that the primary structure of vortex rings will have a large wavelength. The wavelengths of the two other structures are related to this one. Therefore, the identification of the different vortex structures is easier for a measurement system with a given spatial resolution. Nevertheless, the use of a low frequency has a drawback, as the forcing amplitude needed to produce a laterally spreading inner jet has a minimum around $St = 1$ (Rodríguez et al 2000). Therefore, the forcing amplitude in these experiments is very large, and almost approaches unity.

Figure 4 shows the azimuthal vorticity maps and the strain maps for the four equi-spaced phases of the forcing signal. The field of view is not centred with the nozzle axis but displaced downwards. As the nozzle exit lip has 5 azimuthal lobes, the illuminating plane provides with information in two opposite locations of the lobed profile of the nozzle and the minimum location is here of more interest. Flow comes from left to right and the lobes of the nozzle exit lip can be observed, in black, in the left margin. The field of view covers from the upper exit lip ($r = D/2$) to one nozzle diameter below the lower exit lip ($r = 3D/2$). In the axial direction, the field of view covers approximately form $z = 0$ to $z = 3D$.

The first image shows the incipient concentration of a primary vortex ring over the nozzle exit lip. Due to the strong axial forcing and the large wavelength of the primary structure, this process is very similar to the generation of isolated vortex rings, as shown by Didden (see Van Dyke (1982), plate 76). The primary vortex ring development can be seen in the three following images. In the last one, the following vortex ring can also be observed, emerging from the nozzle exit. But this new vortex ring appears associated with a previous concentration of counter-rotating vorticity. This new vortex is of paramount importance in the flow evolution. Its origin can be explained coming back to the parallelism with isolated vortex rings. The images in plate 76 of Van Dyke (1982) show how, as the vortex ring leaves the nozzle, it induced a secondary vortex ring of opposite circulation. This mechanism can also be related to the fulfilment of an unsteady Kutta condition in the nozzle lip, a problem addressed by Crighton (1985).

The counter rotating vortex ring instantaneously falls under the influence of the forming primary vortex ring. As the flow develops, from image 1 to 4, the vorticity maps show how the induction of this forming vortex ring displaces and deforms the counter-rotating vortex ring, which circulation is smaller. The process ends up with the lateral ejection of parts of this counter-rotating ring, which begin to drift at the outer flow velocity. This last evolution is only fulfilled in azimuthal positions aligned with the minima of the lobed nozzle lip, as observed by Rodríguez et al (2000).

The information of the strain field is of importance in understanding the evolution of the counter-rotating vortex ring. The maps show that the strain is large in zones of concentrated vorticity and considerable in the surroundings of the primary vortex ring. Comparing the information with that of the vorticity maps, one can see that the counter-rotating ring moves in a region of considerable strain. A strain field can cause to effects over a vortex, depending on their relative direction. For an azimuthal structure, the strain presented here will cause a deformation of the internal structure of the vortex. But if the structure is of semi-axial vorticity, the strain field will re-direct it in the axial direction and produce a concentration of its vorticity following the Lin and Corcos (1984) mechanism. Therefore, the actual azimuthal organisation of the counter-rotating vortex ring is of paramount importance. Hence, it should be considered that in the moment of its concentration on the nozzle lip, the structure is a quasi-axisymmetric ring. Nevertheless, the azimuthal perturbation imposed by the lobed nozzle must produce a slight azimuthal variation. This azimuthal waviness will be strongly enhanced by the observed strain field and the counter-rotating vortex ring will develop a highly-stretched, highly-bent wavy shape.

This complex evolution is difficult to observe in the longitudinal cuts presented in this work, as the axial vorticity was not measured. Nevertheless, it can be noted that initially the counter-rotating ring is defined by a point concentration of counter-rotating vorticity, which can be seen in blue, at the nozzle exit in image 4. But in its further stages, the counter-rotating vortex evolves into a row of accumulations of vorticity of both signs (image 2, 3), which can be understood as cuts of a semi-axial distorted vortex.

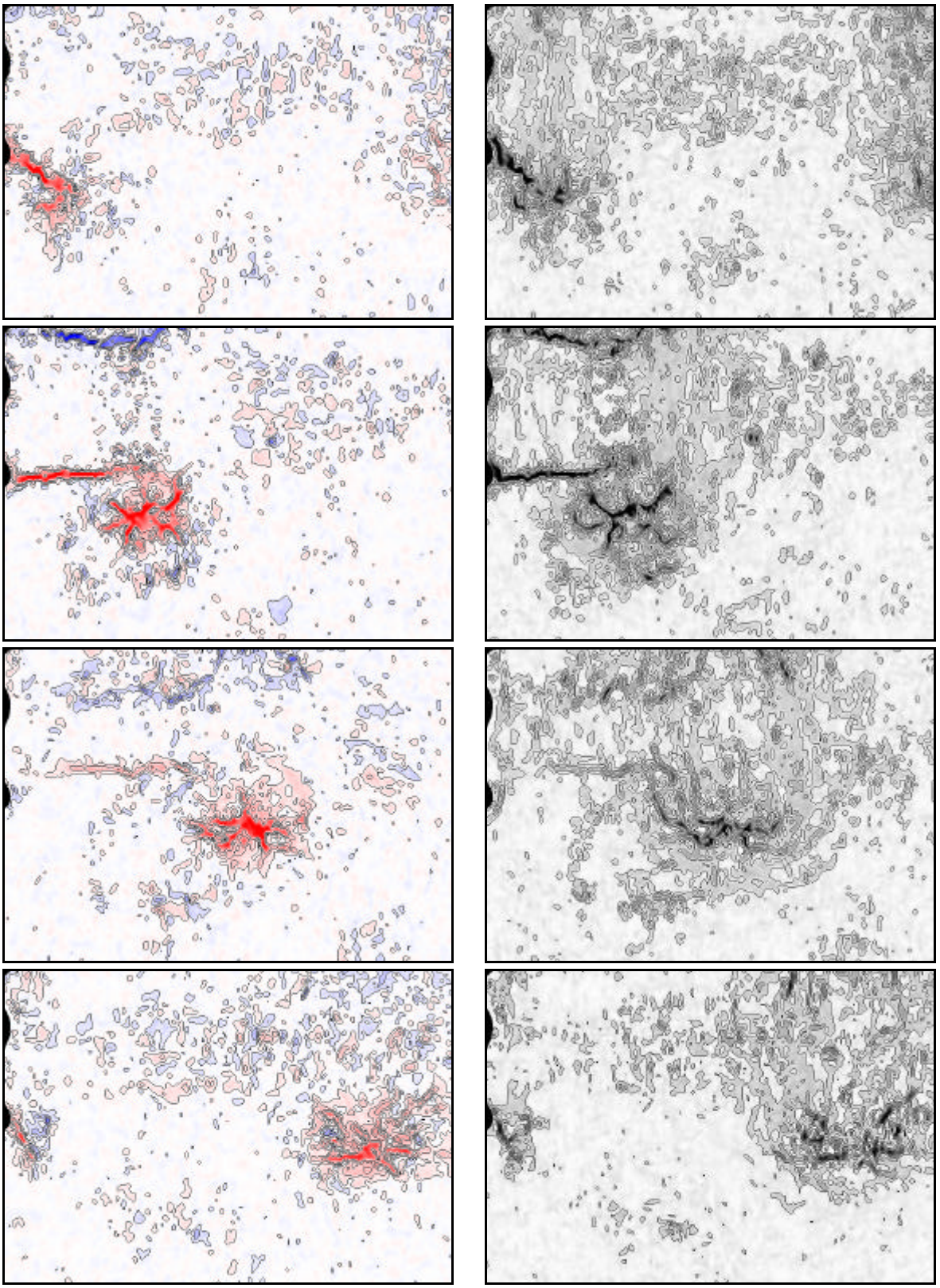

a) Azimuthal vorticity

b) Strain

-10^3 0 $10^3 \cdot s^{-1}$ 0 $5 \cdot 10^2$ $10^3 \cdot s^{-1}$

Figure 4. *Vorticity and strain field calculated from four DPIV velocity maps. Phases equi-spaced along a forcing cycle. Flow comes from left to right. The nozzle exit lobes can be seen on the upper left side.*

Coming back to the primary vortex ring, it is interesting to draw attention on its core structure. The vorticity is here organised in filaments distributed along the core. The usual description of the vortex core shows a Gaussian distribution of the vorticity inside the core. Nevertheless, this description is obtained with statistical measurements such as LDV. This is coherent to the distribution that could be obtained if several phase-lock PIV measurements are averaged, as the position of the filaments will slightly differ from one record to another. Anyway, the validation of the core structure observed in the vorticity maps is complex. The measurement system resolution is well below the wavelength of the structure, but slight differences between the movement of the seeding particles and the flow cannot be neglected.

The information of figure 4 may be better understood if the local values of the strain and the azimuthal vorticity are compared. Figure 5 represents a local parameter that gives such comparison. The local coefficient, χ, is calculated following eq. (4).

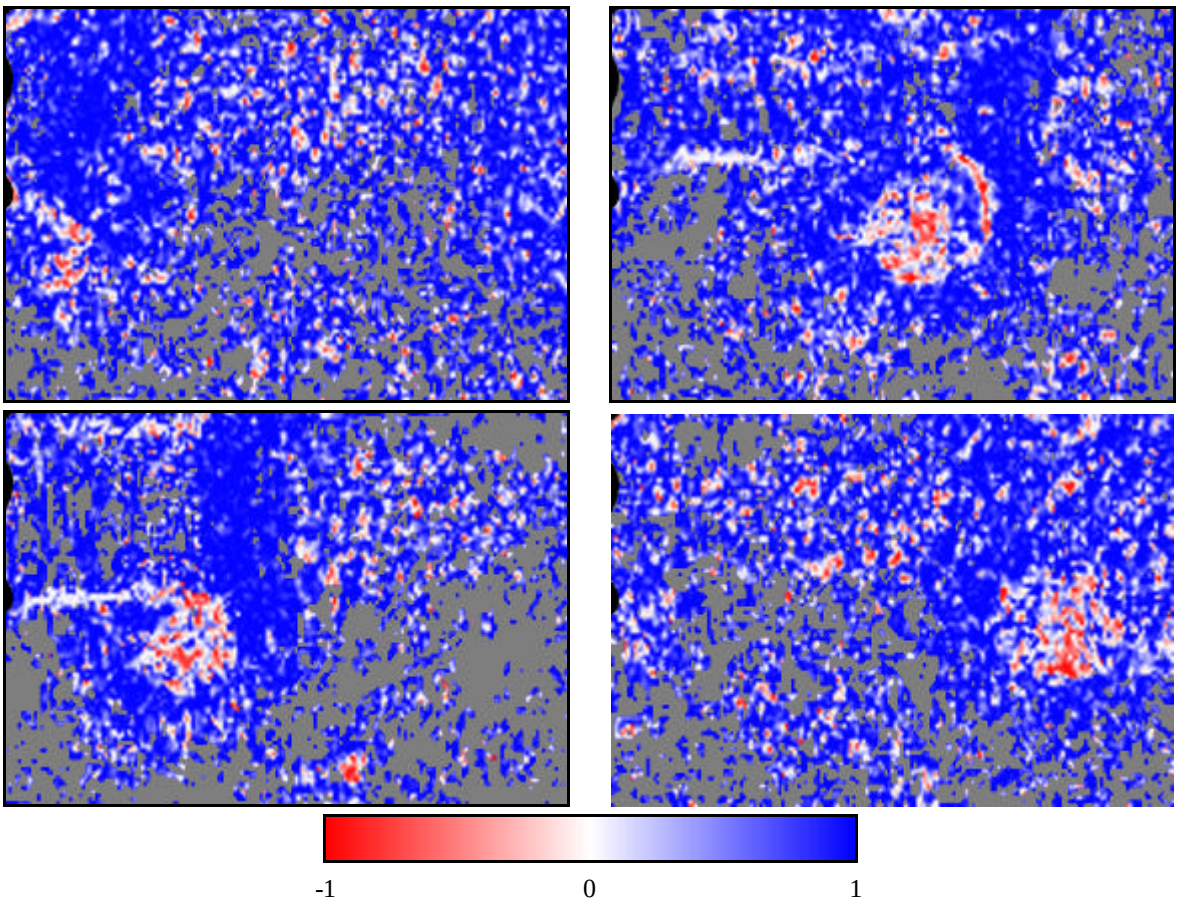

Figure 5. *Local coefficient between azimuthal vorticity and strain calculated from four DPIV velocity maps. Phases equi-spaced along a forcing cycle. Flow comes from left to right. The nozzle exit lobes can be seen on the upper left side. The grey zones indicate zones were both the vorticity and the strain are negligible.*

Four zones can be distinguished, following the work of Tanaka and Kida (1993) depending on the value of the local coefficient. The zones in red represent positions were $\chi \approx -1$, and thus the vorticity is dominant. These locations represent the vortices and include the evolving primary vortex ring core, the stretched counter-rotating vortex and some residual vorticity in the remaining shear layer on the braids. The zones in blue represent positions were $\chi \approx 1$, and thus the strain is dominant. These locations represent deformation cells and include the surroundings of the primary vortex ring and its inner front. The zones in white represent positions were $\chi \approx 0$, and thus the vorticity and strain are balanced. These locations, when concentrated, represent vortex sheets. Here, the initial shear layer behind the evolving primary ring has such condition in images 2 and 3, before the vortex moves further downstream. Finally, the specific problem of this local coefficient is that it do not distinguish between

zones were either the strain, the azimuthal vorticity or both are small or large. Thus, the information when both parameters are residual is unimportant and may induce errors of appreciation. Therefore, the information is ignored on locations were the sum of the squares of both parameters is less than 10% of the mean sum of squares in the total field of view. Such locations are seen in grey.

Finally, the pressure distribution can be obtained using eq. (5). Figure 6 presents the calculated values of the Laplacian of pressure for the four phases presented. The regions of high pressure are defined by large negative values of the Laplacian, which suggest the existence of a maximum of pressure. Such zones are related to zones of high strain (deformation cells). The regions of low pressure are defined by large positive values of the Laplacian, which suggest the existence of a minimum of pressure. Such zones are related to zones of high vorticity (vortex cores).

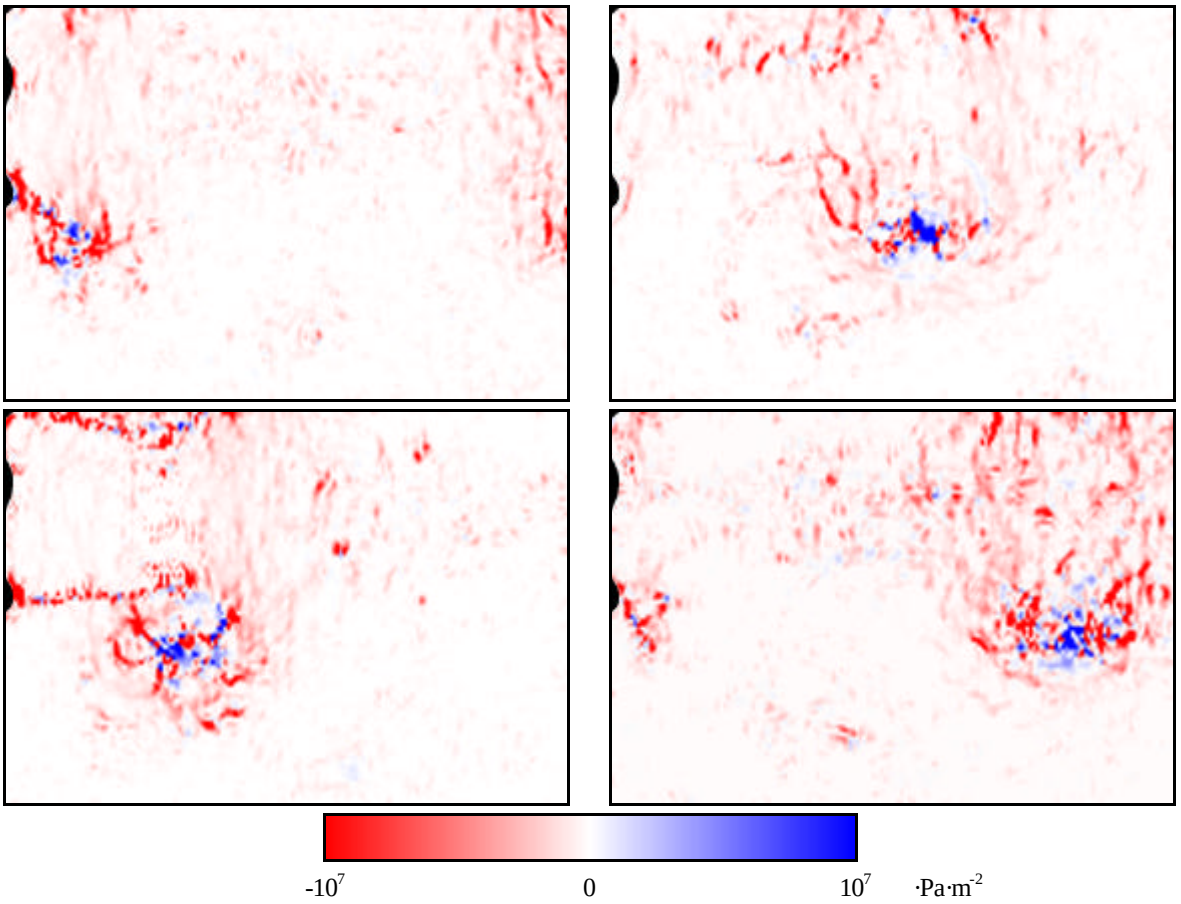

Figure 6. *Laplacian of the pressure calculated from four DPIV velocity maps. Phases equi-spaced along a forcing cycle. Flow comes from left to right. The nozzle exit lobes can be seen on the upper left side.*

The experimental evidence presented here validates the qualitative explanation of the vortex evolution of Rodríguez et al (2000) Figure 7 presents a sketch of the near-field vortex motions suggested in that previous article, that bases its reasoning in inviscid processes. The graph includes the secondary structure usually present in all shear layers, a structure that cannot be observed in the measurements presented here, being a structure of axial vorticity. Note that the evolution of the counter-rotating vortex ring and its lateral motion is well-described in the graph.

5. CONCLUSIONS

The near-field vortex dynamics of transitional co-flowing jets in which the inner jet is strongly forced is studied. Several phase lock measurements of two components of the velocity vector in a diametrical plane of the flow are obtained using the 2D DPIV technique, and the azimuthal vorticity and the strain fields are derived. The results show the evolution of the two structures of azimuthal vorticity that develop in the flow. It is shown that the

vortex dynamics in the near-field can be reduced to the inviscid mechanisms described by Rodríguez et al (2000). The coupled information of the vorticity and strain fields allows to identify the vortex structure and the zones of deformation and stretching.

The use of a high-resolution PIV algorithm allows the identification of the small-scale vortex structures and provides with information about the core structure of the vortices.

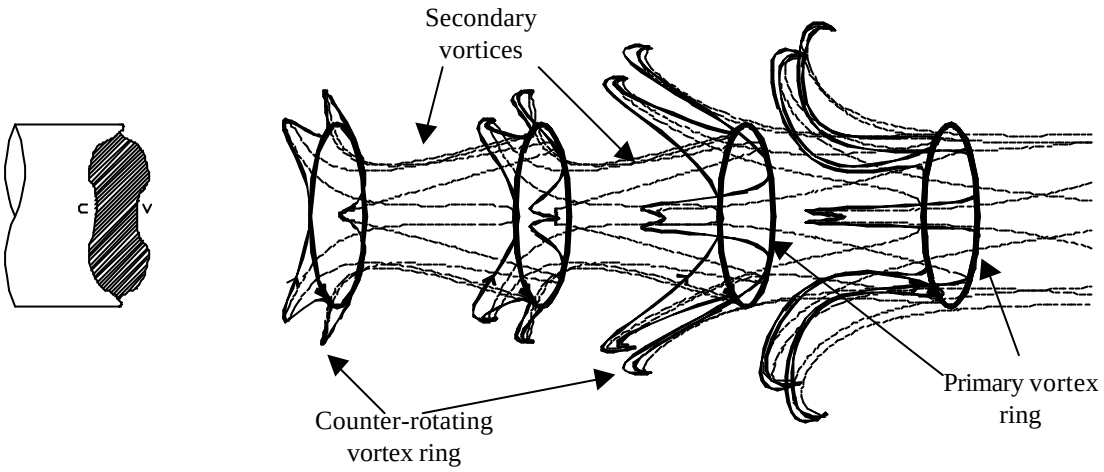

Figure 7. *Qualitative description of the near-field vortex dynamics for the high forcing amplitude case.*

REFERENCES

Bradshaw, P. & Koh, Y.M. 1981. *A note on Poisson's equation for pressure in a turbulent flow*. Phys. Fluids 24, p. 777.

Brancher, P., Chomaz J. & Huerre, P. 1994. *Direct numerical simulations of round jets: vortex induction and side jets*. Phys. Fluids 6, p. 1768-1774.

Crighton, D.G. 1985. *The Kutta condition in unsteady flow*. Annu. Rev. Fluid Mech. 17, p. 411-445.

Grinstein, F., Gutmark, E., Parr, T., Hanson-Parr, D. & Obeysekare, U. 1996. *Streamwise and spanwise vortex interaction in an axisymmetric jet*. Phys. Fluids 8, 6, p. 1515-1524.

Lasheras, J.C., Liñán, A., Lecuona, A. & Rodríguez, P. 1992. *Vorticity dynamics in three dimensional pulsating co–flowing jet diffusion flames*. 24th Symposium on Combustion, p. 325-332.

Lin, S. J. & Corcos, G. M. 1984. *The mixing layer - Deterministic models of a turbulent flow. III - The effect of plane strain on the dynamics of streamwise vortices*. J. Fluid Mech. 141, p. 139-178.

Monkewitz, P.A. & Pfizenmaier, E. 1991. *Mixing by 'side jets' in strongly forced and self-excited round jets.* Phys. Fluids 3, 2, p. 1356-1361.

Nogueira, J., Lecuona, A. & Rodríguez, P. 1999. *Local field correction PIV: on the increase of accuracy of digital PIV systems*. Exp. Fluids 27, p. 107-116.

Rodríguez, P., Ruiz-Rivas, U. & Lecuona A. 2000. *Near field vortex dynamics in axially forced, laminar, co-flowing jets: A descriptive study of the flow configurations.* Sent to European J. Fluid Mech. B/Fluids. Also Ruiz-Rivas, U., Lecuona, A. & Rodríguez, P. 2000. *Near field vortex dynamics in axially forced, co-flowing jets: Quantitative description of a low-frequency configuration.* In preparation.

Tanaka, M. & Kida, S. 1993. *Characterization of vortex tubes and sheets*. Phys. Fluids A, 5, 9, p. 2079-2082.

Van Dyke, M. 1982. *An album of fluid motion*. The Parabolic Press, Stanford, California.